Interaction Between Closely Packed Array Antenna Elements Using Metasurface for Applications Such as MIMO Systems and Synthetic Aperture Radars

Mohammad Alibakhshikenari[1]*, Bal S. Virdee[2], Panchamkumar Shukla[2], Chan H. See[3], Raed Abd-Alhameed[4], Francisco Falcone[5], and Ernesto Limiti[1]

[1] Electronics Engineering Department, University of Rome "Tor Vergata", Via del Politecnico 1, 00133, Rome, ITALY
[2] London Metropolitan University, Center for Communications Technology, School of Computing & Digital Media, London N7 8DB, UK
[3] School of Engineering, University of Bolton, Deane Road, Bolton, BL3 5AB, UK
[4] School of Electrical Engineering & Computer Science, University of Bradford, UK
[5] Electric and Electronic Engineering Department, Universidad Pública de Navarra, SPAIN
* alibakhshikenari@ing.uniroma2.it

Abstract: The paper presents a technique to enhance the isolation between adjacent radiating elements which is common in densely packed antenna arrays. Such antennas provide frequency beam-scanning capability needed in Multiple-Input Multiple-Output (MIMO) systems and Synthetic Aperture Radars (SARs). The method proposed here uses a metamaterial decoupling slab (MTM-DS), which is located between radiating elements, to suppress mutual-coupling between the elements that would otherwise degrade the antenna efficiency and performance in both the transmit and receive mode. The proposed MTM-DS consists of mirror imaged E-shaped slits engraved on a microstrip patch with inductive stub. Measured results confirm over 9–11 GHz with no MTM-DS the average isolation (S_{12}) is -27 dB; however, with MTM-DS the average isolation improves to -38 dB. With this technique the separation between the radiating element can be reduced to $0.66\lambda_o$, where λ_o is free space wavelength at 10 GHz. In addition, with this technique there is 15% improvement in operating bandwidth. At frequencies of high impedance match of 9.95 GHz and 10.63 GHz the gain is 4.52 dBi and 5.40 dBi, respectively. Furthermore, the technique eliminates poor front-to-back ratio encountered in other decoupling methods. MTM-DS is also relatively simple to implement. Assuming adequate space is available between adjacent radiators the MTM-DS can be fixed retrospectively on existing antenna arrays, which makes the proposed method versatile.

Keywords: Metamaterial decoupling slab (MTM-DS), antenna arrays, frequency beam-scanning, synthetic aperture radars (SAR), multiple-input multiple-output (MIMO) systems.

I. INTRODUCTION

With the advent of 5G mobile communications multiple-input multiple-output (MIMO) systems are expected to play a major role. This is because MIMO antennas provide advantages of increased data rate, reliability, quality, and channel capacity. Moreover, MIMO system can mitigate the effects of multipath fading. However, one of the main challenges in the design of MIMO antennas is isolation reduction between adjacent closely spaced antennas with a spacing of less than a wavelength at the operating frequency. Suppressing the coupling between radiating elements in MIMO reduces degradation in the corresponding impedance and radiation properties [1]-[3]. Mutual coupling also encountered in antenna arrays is mainly attributed to three factors, i.e. (i) signal leakage via surface waves along the substrate; (ii) coupling between the feedlines through conducting current on the metallic background; and (iii) coupling due to the spatial electromagnetic fields [1]. Surface waves have a significant impact on the mutual coupling when microstrip substrate thickness h is greater than $0.3\lambda_o/(2p/\sqrt{\varepsilon_r})$ [4], where λ_o is the operating wavelength in free space, p is a positive integer and ε_r is the relative permittivity of the dielectric substrate. Surface wave coupling diminishes only by 3 dB when the distance between the antennas is doubled. Over recent years numerous techniques have been proposed to reduce the mutual coupling between antenna radiating elements in the design of antenna arrays. In [5][6], shorted patches have been used to negate excitation of the surface wave modes. In [7], electromagnetic bandgap (EBG) structures are employed to suppress mutual coupling. Defected ground structures (DGS) have also been investigated to suppress mutual coupling [8]. In fact, DGS resonators have been used in various applications including microwave filters and matching circuits as well as suppressing harmonic and cross-polarisation in microstrip antennas [9]-[11]. Compared with EBG structures, the advantage of DGS is that it can be used to realize bandgap effect with a more compact circuit size. In [12] mutual coupling is suppressed by 14 dB in a densely packed antenna by using metamaterial structures etched in the ground plane and the top layer; however, the antenna's front-to-back ratio is poor. In a recent work, side-lobe suppression of 4.3 dB has been achieved using complementary split-ring resonator (CSRR) loading in the ground plane of antenna array [13]. Use of slot combined CSRR structure etched in the ground plane and on the top layer of the antenna array is shown to provide coupling suppression of 19 dB [14]. With this technique, however, the front-to-back ratio is deteriorated. Other coupling suppression techniques using metamaterial or EBG suffer from either complex fabrication process or large separation between radiating elements [15]-[18].

In this paper, mutual coupling between radiating elements is reduced significantly using metamaterial decoupling slab (MTM-DS) in closely packed antenna arrays that are used in MIMO and synthetic aperture radar (SAR) systems. In the proposed technique, the MTM-DS is deployed between the radiating antennas. MTM-DS can be applied retrospectively subject to sufficient spacing between the radiating elements, which makes the technique versatile. With this technique the edge-to-edge separation between the radiators can be reduced to $0.66\lambda_o$, where the free space wavelength is at 10 GHz. Measured results confirm the mutual coupling between the antennas is suppressed on average by 38 dB from 9 GHz to 11 GHz. The paper is organised as follows. In section II, the antenna array without MTM-DS is first characterised and its simplified equivalent circuit model is presented. Next, the metamaterial decoupling slab is characterised and applied in the antenna array. This structure's equivalent circuit model is compared with the full-wave electromagnetic model. Decoupling effect by the proposed MTM-DS is next confirmed using surface current plots over the antenna array. In section III, parametric study on the MTM-DS is performed to gain an insight of how the physical parameters of the structure affect its performance. Measured and simulated results of the antenna array without and with MTM-DS are presented in section IV. The radiation patterns of the antenna array are given in section V along with comparison with other techniques reported to date. The work is concluded in section VI.

II. ANTENNA DESIGN

A) Antenna Array with No MTM-DS

Structure of 2×1 element microstrip patch, which constitutes the unit cell of an antenna array is shown in Fig. 1 where the waveguide ports are applied to the feedlines for simulation purpose. The ground plane is truncated to enhance the impedance bandwidth of the two-element antenna array. Individual patch antennas are modelled as parallel *RLC* resonant circuits whose radiation impedance is function of feedline position. The two identical patch antennas have dimensions L = 35 mm and W = 30 mm.

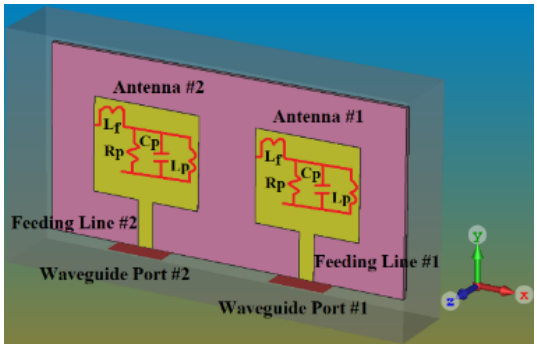

(a) Isometric view of the patch antennas. The equivalent circuit model is annotated, where L_f represents the feedline inductance, R_p the patch resistance, C_p the patch capacitance, and L_p the patch inductance.

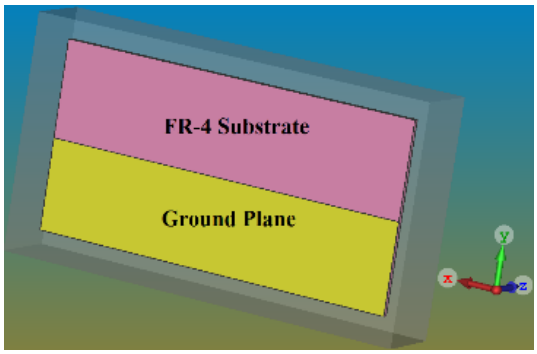

(b) back view (ground plane)

Fig. 1. Configuration of 2×1 antenna array constructed on FR-4 lossy substrate with thickness of h = 1.6 mm, dielectric constant of $\varepsilon_r = 4.3$ and $tan\delta = 0.025$.

Input impedance of each microstrip patch antenna, shown in Fig. 2, was computed using 3D full-wave EM simulation tool, i.e. CST Microwave Studio. In the simulation, all the boundary conditions were specified as "open (added space)" which assumes that no external conditions are applied to the antenna. Under this condition the simulator effectively places perfectly matched microwave absorber material at the boundary, which guarantees the antenna array is in open space.

The equivalent circuit model parameters given in Table I were extracted using optimization method in CST Microwave Studio over a specified frequency range. This is the reason why the mapping is coherent.

The simulated reflection and transmission coefficient response of the antenna array as a function of gap (d) between the antennas is shown in Fig. 3. Coupling behaviour between the two identical patches in Fig. 1 was also analysed. In the analysis the ground plane was represented as a perfect electric conductor (PEC) boundary. Coupling coefficient was extracted from the transmission coefficient response of the structure. Frequency of the resonance peaks corresponding to the two patches, i.e. f_1 and f_2, were used to determine the coupling coefficient k_{12} using the following relation [19]

$$k_{12} = \frac{f_2^2 - f_1^2}{f_2^2 + f_1^2} \qquad (1)$$

Coupling coefficient is plotted in Fig. 3(c) as a function of the gap (d) between the patches. It shows the coupling coefficient reduces linearly with increasing the gap between the patches.

TABLE I: Extracted Parameters Representing the Equivalent Circuit Model of the Patch Antenna (Lumped elements are annotated in Fig.1).

Parameters	R_p	C_p	L_p	L_f
Value	55Ω	15.9 pF	0.2 nH	2 nH

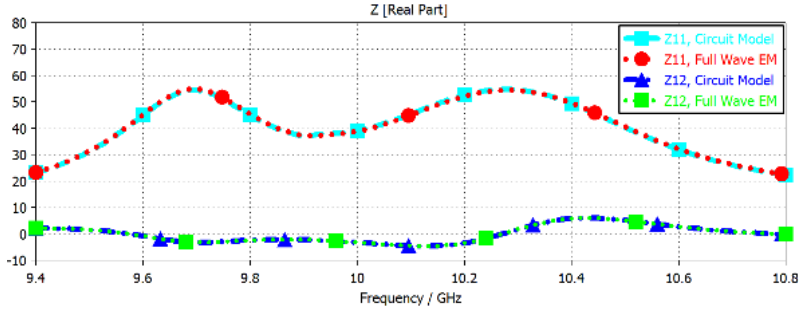

(a)

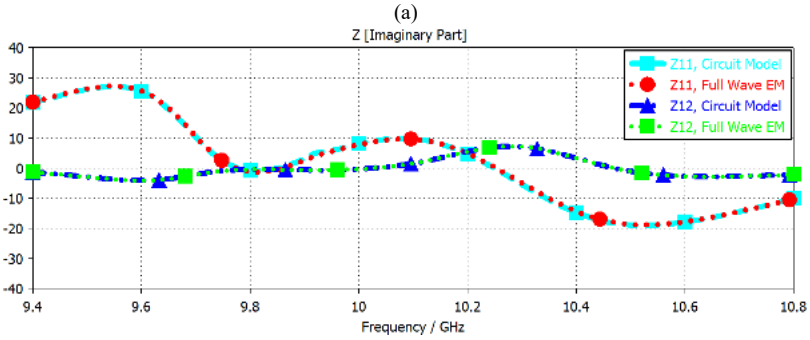

(b)

Fig. 2. Input impedances (Ω) of a single antenna element.

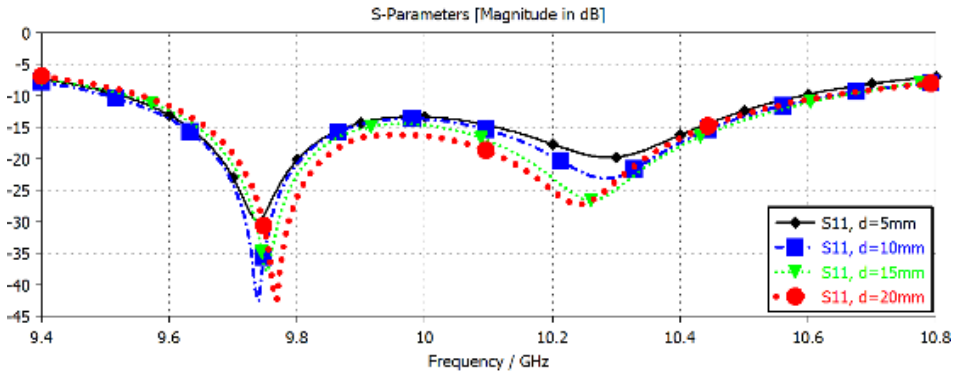

(a)

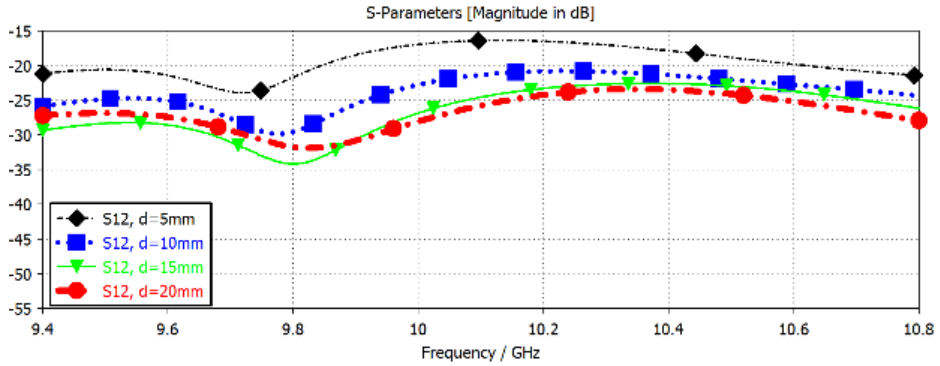

(b)

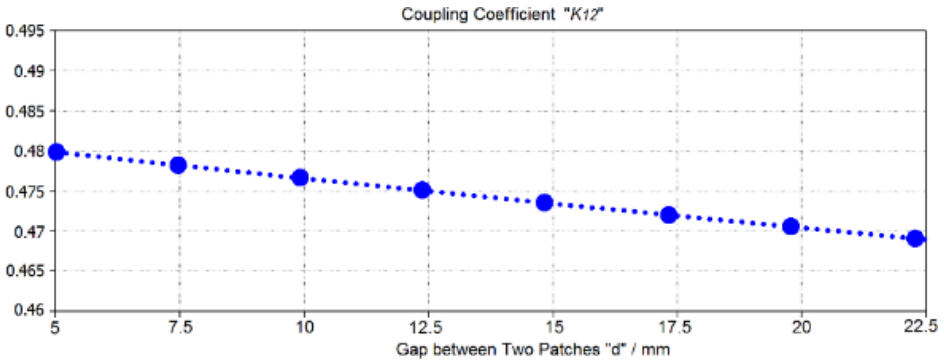

(c)

Fig. 3(a)-(b). Reflection and transmission coefficient response, and (c) coupling coefficient as a function of gap between the two patches.

The simplified equivalent circuit model of the two-element patch antenna array is shown in Fig. 4. Electromagnetic coupling between the two patches is represented by coupling coefficient k_{12}. Microstrip patches are represented by parallel *RLC* resonant circuit whose values are given in Table II. As the two antennas are identical the magnitude of their characterising parameters is the same. Fig. 5 shows the circuit model response matches exactly with the full-wave EM simulation response. This figure shows that the proposed array operates over 9.56 GHz – 10.63 GHz, with bandwidth of 1.07 GHz and fractional bandwidth of 10.6%. In addition, impedance matching is particularly good at two resonance frequencies of $f_{r_1} = 9.76$ GHz and $f_{r_2} = 10.24$ GHz. At these frequencies the isolation between elements is S_{12}= -31 dB and -24 dB, respectively.

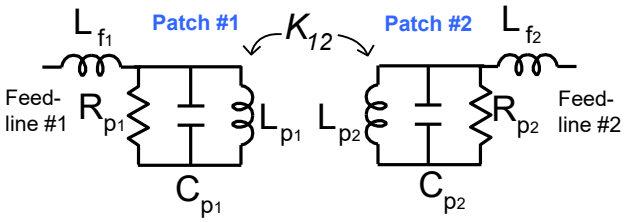

Fig. 4. Equivalent circuit model of two-element basic antenna array of Fig. 1.

TABLE II: Equivalent Circuit Parameters of the Two-Element Antenna Array Antenna in Fig. 4.

Parameters	Value
R_P	55 Ω
C_P	16.2 pF
L_P	0.2 nH
L_F	2.2 nH
K_{12}	0.047

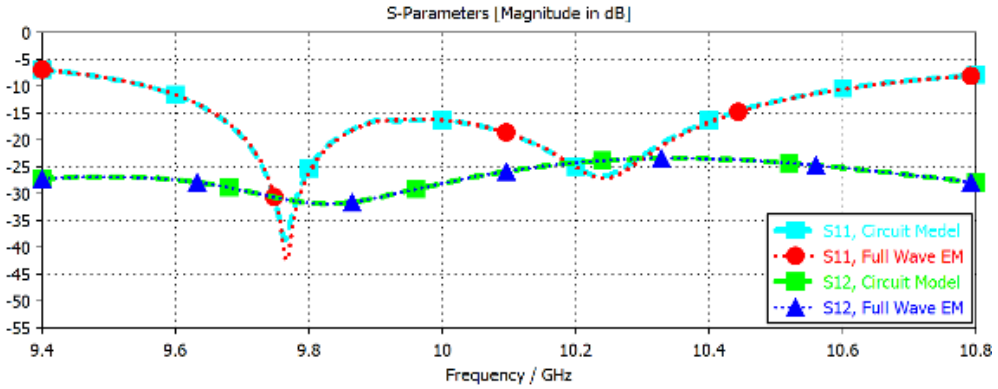

Fig. 5. Reflection and transmission coefficient response (S_{11} and S_{12}) of the proposed two element antenna array.

B) *Metamaterial Decoupling Slab*

Metamaterial property of negative permeability and permittivity exhibited by slotted patch antenna is well established and described in detail in [20]-[22]. Structure of the MTM-DS proposed here, which is shown in Fig. 6, was determined from simulation analysis. It consists of two E-shaped slits that are etched in a rectangular microstrip patch with a high impedance open-circuited stub at the bottom. The E-shaped slits are arranged as a mirror image. The E-shaped slits are essentially capacitive in nature, and the high impedance stub of quarter wavelength length acts like grounded inductance. The equivalent electrical circuit of the decoupling slab corresponds to that of a metamaterial structure [23]. As the proposed MTM-DS configuration is free of metal vias its fabrication is considerably economic. MTM-DS was fabricated on the same substrate as the patch elements, i.e. FR-4 lossy substrate of 1.6 mm thickness and dielectric constant of 4.3. Optimized dimensions of the MTM-DS structure are given in Table III.

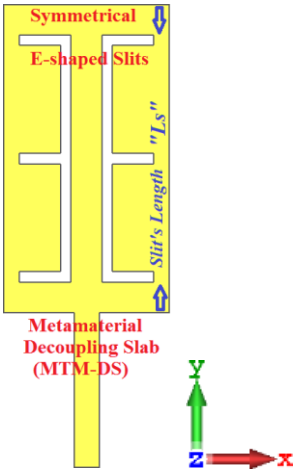

Fig. 6. The structure of the proposed metamaterial decoupling slab, where surface waves propagate along the *x*-axis, H||*y*, E||*z*.

Constitutive parameters, i.e. permittivity and permeability, of MTM-DS were calculated from the scattering parameters of the structure using the technique proposed by Smith *et al.* [24]. Scattering parameters, permittivity and permeability of the MTM-DS structure are plotted in Fig. 7 as a function of slot length (*Ls*). The resonator exhibits negative permittivity ($\varepsilon < 0$) and negative permeability ($\mu < 0$) in regions of the frequency spectrum confined between 8 GHz to 12 GHz, which is characteristic if metamaterials. The E-shaped slits enable fine tuning of the structures resonant frequency without varying other parameters.

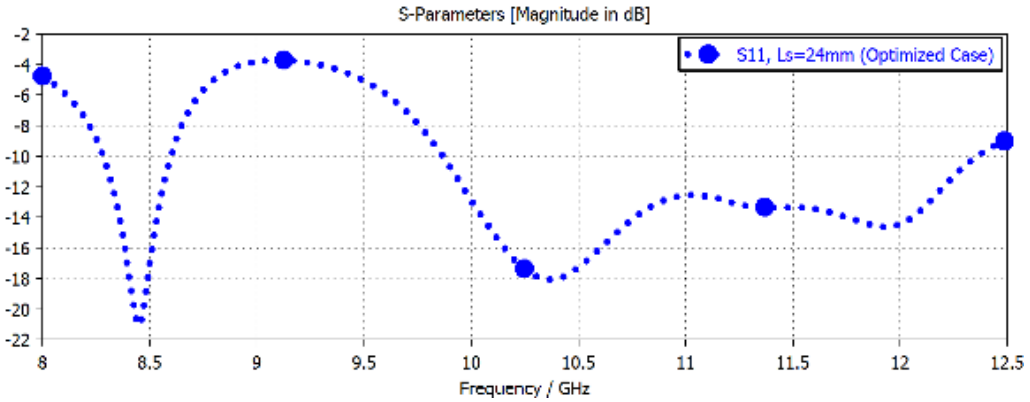

(a)

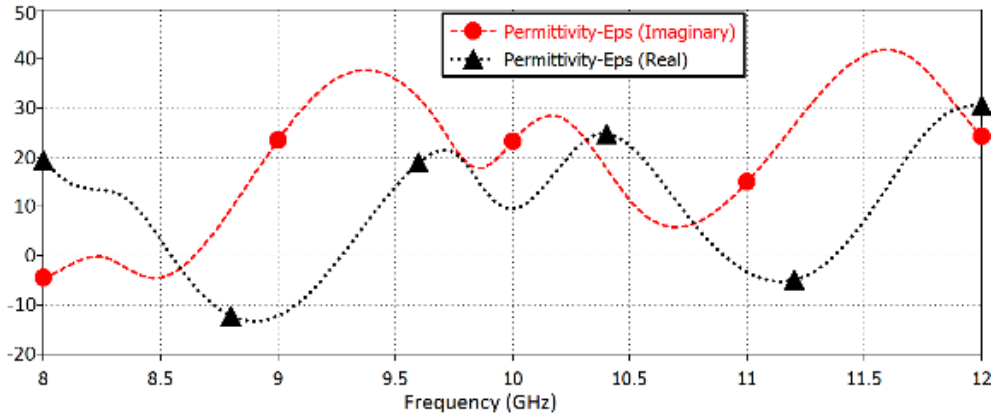

(b)

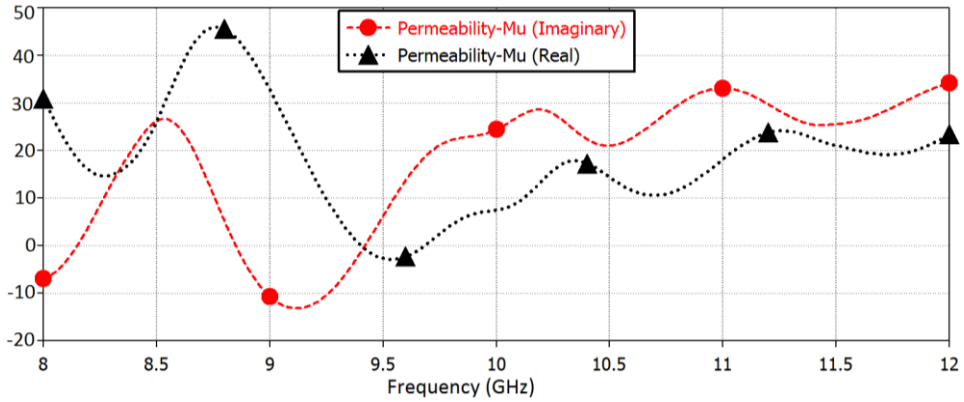

(c)

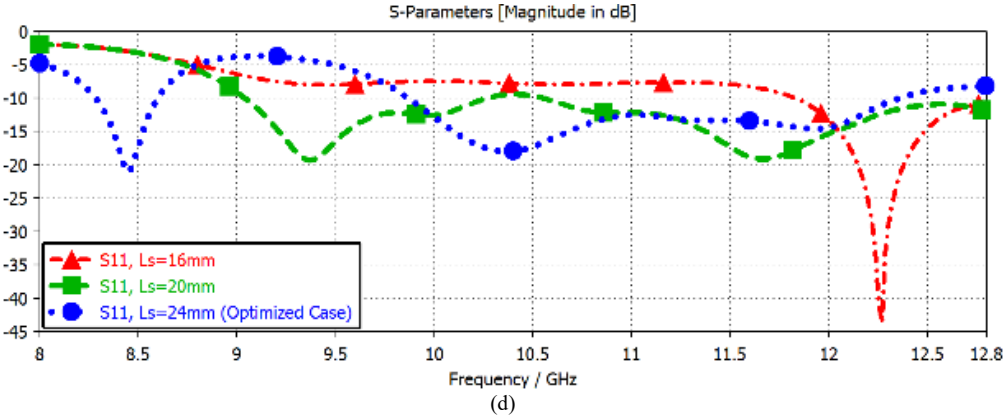

(d)

Fig. 7. MTM-DS response: (a) S_{11}, (b) permittivity (Eps), (c) permeability (Mu), and (d) S_{11} as a function of slit length (*Ls*).

C) Planar Antenna Array with MTM-DS

MTM-DS was incorporated in the patch antenna array, as shown in Fig. 8, and fabricated on the same substrate that was specified earlier. Microstrip stub attached to the MTM-DS is an open circuit. Dimensions of the radiation patches and MTM-DS are 35×30 mm^2 and 16×30 mm^2, respectively. The edge-to-edge separation between the radiating patch elements is $0.66\lambda_o$, where λ_o is free space wavelength at 10 GHz. Each patch is individually fed by a microstrip feedline. The dimensions of the structure in Fig. 8 are given in Table III.

1) Equivalent Circuit Model: In Fig. 8 the E-fields are polarized along *z*-axis and the coupling between the patches is along the *x*-axis. The simplified equivalent circuit model of the two-element radiating patch antenna with metamaterial decoupling slab is shown in Fig. 9, where the patches and MTM-DS are represented as parallel *RLC* circuit. Coupling between patch#1 and decoupling slab is represented by K_{DS1}; and the coupling between patch#2 and decoupling slab is represented by K_{DS2}. The extracted equivalent circuit parameters of Fig. 9 are given in Table IV. Comparison of the equivalent circuit and 3D full-wave EM simulation model responses are shown in Fig. 10. S-parameters of the 2×1 array antenna without and with MTM-DS is shown in Fig. 11.

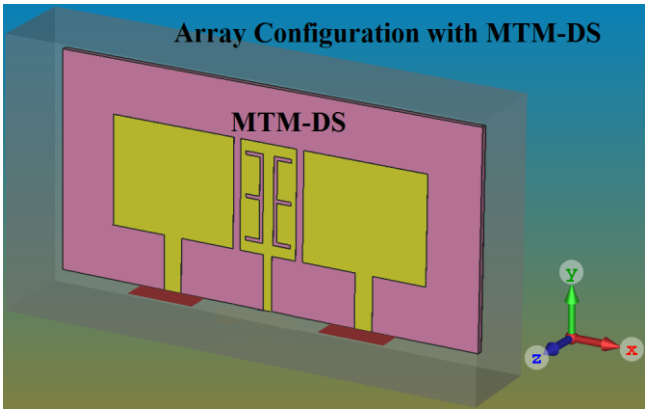

(a)

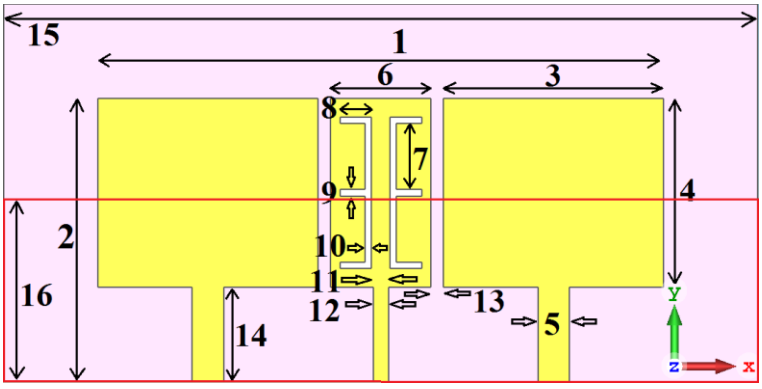

(b)

Fig. 8. Geometry of 2×1 antenna array with MTM-DS, (a) isometric view, and (b) numerical labels define the geometry of the antenna array and MTM-DS are given in Table III.

TABLE III: Dimensions (in mm) of 1×2 Antenna Array with MTM-DS

#1	#2	#3	#4	#5	#6	#7	#8
57.58	25.17	18.77	16.43	2.13	8.96	5.3	2.77

#9	#10	#11	#12	#13	#14	#15	#16
0.52	0.52	1.71	1.28	5.54	8.53	67.41	16.21

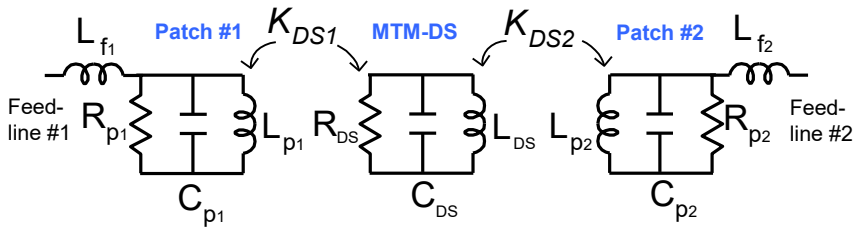

Fig. 9. Simplified equivalent circuit of two-element radiating patch with MTM-DS.

TABLE IV: Elements Values for Two Element Array Antenna with MTM-DS.
Parameters of the two radiating patches are identical including K_{DS1} and K_{DS2}.

Parameters	L_F	R_P	C_P	L_P	K_{DS}	R_{DS}	C_{DS}	L_{DS}
Value	2.2 nH	55 Ω	16.2 pF	0.2 nH	0.0095	2200 Ω	2.25 pF	1.5 nH

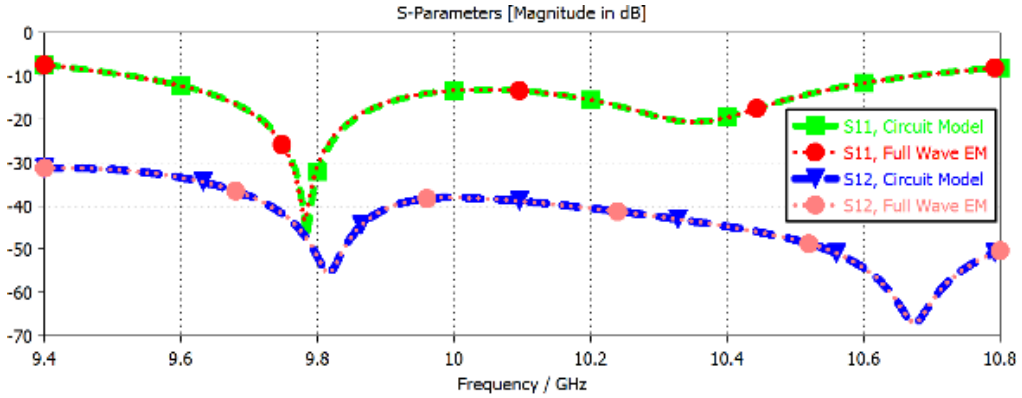

Fig. 10. Comparison of S-parameter response of the circuit and EM models for the 2×1 antenna array with MTM-DS.

Fig. 11 reveals that when MTM-DS is inserted in the middle of the two radiating elements it introduces transmission zeros at 9.81 GHz and 10.65 GHz, resulting in significant mutual coupling suppression of -55 dB and -67.50 dB, respectively. MTM-DS has effectively improved the mutual coupling suppression at the two notch frequencies by 24 dB and 43.57 dB, respectively. The performance of antenna array without and with MTM-DS is summarized in Table V.

Decoupling effects can also be observed by visualizing the surface current density plots over the 2×1 antenna array. With MTM-DS strong currents are induced on the patch antenna, as shown in Fig. 12, which clearly verifies the effectiveness of the MTM-DS in suppressing surface current wave interaction between the two patches.

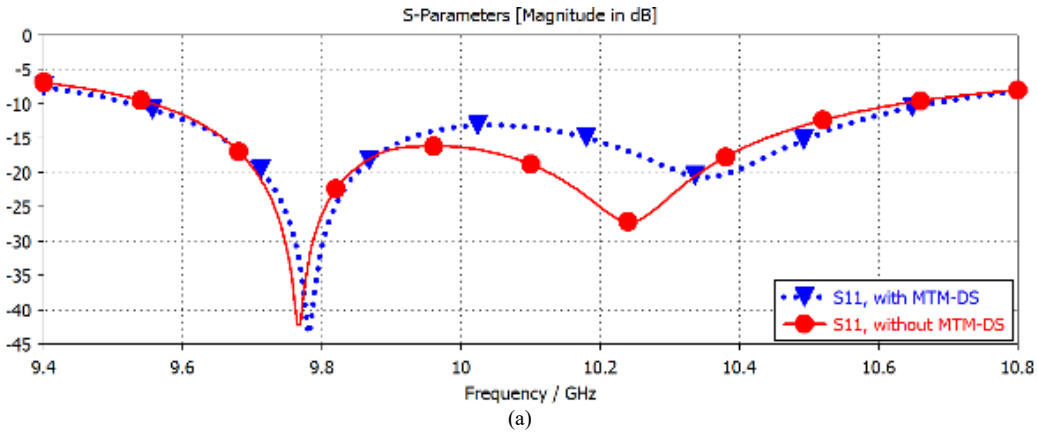

(a)

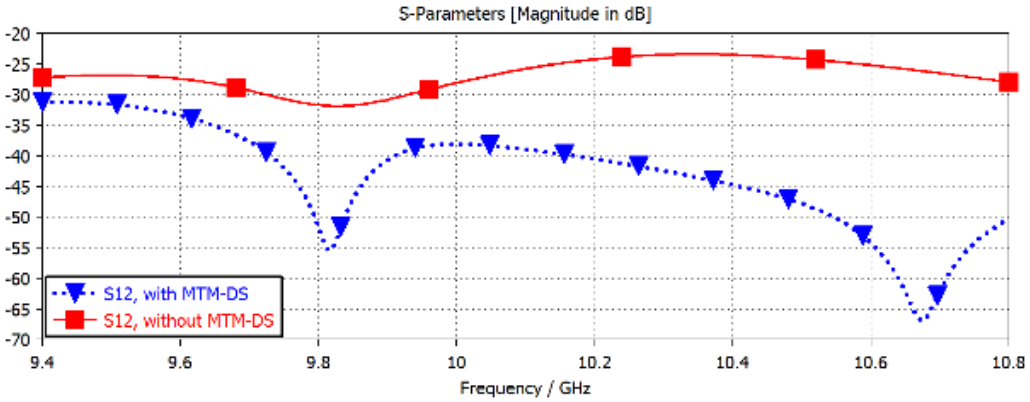

(b)

Fig. 11. S-parameter response of 2×1 antenna without and with MTM-DS antenna array.

TABLE V: Two-Element Antenna Array Without and With MTM-DS.

Case	Operating freq. range (GHz)	Bandwidth (GHz) for S_{11}≤-10 dB	Fractional bandwidth (%)	Notch freq.#1	Notch freq.#2
				Impedance match (dB)	Impedance match (dB)
Without MTM-DS	9.56 – 10.63	1.07	9.43	-42.17	-27.15
With MTM-DS	9.52 – 10.67	1.15	8.78	-43.23	-20.57

Isolation (S_{12})

Case	@ Notch freq.#1	@ Notch freq.#2
Without MTM-DS	-30.97 dB	-23.93 dB
With MTM-DS	-55 dB	-67.50 dB

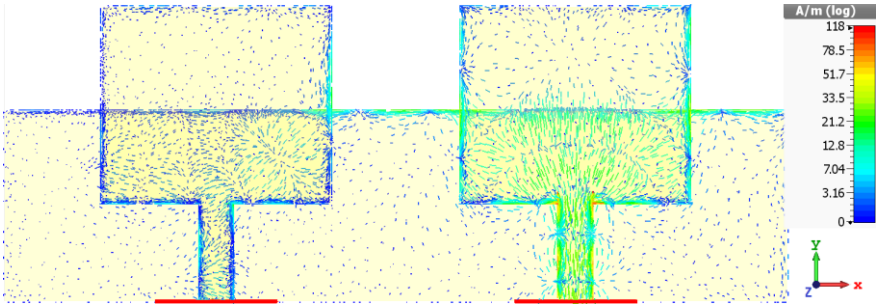

(a) without MTM-DS

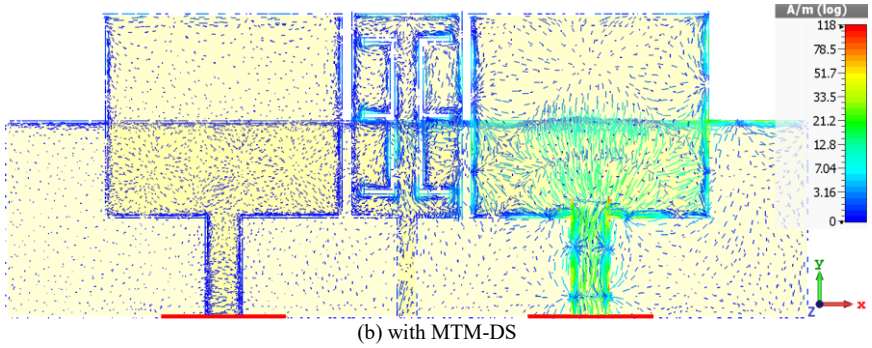

(b) with MTM-DS

Fig. 12. Surface current density plots to validate the effect of MTM-DS at 10.65 GHz.

III. Parametric Study on Metamaterial Decoupling Slab

In this part a parametric study is presented on the proposed metamaterial decoupling slab to understand the effects of the E-shaped slits on the array's performance. The following sections describe the influence of E-shaped slit width and the gap between the slits.

A) Effect of Width of Slits

The influence of width of E-shaped slits (W_1) on reflection and transmission coefficients (S_{11} and S_{12}) is shown in Fig. 13. It is evident that when W_1 is increased from 0.5 mm to 1.25 mm the antenna's reflection coefficient or impedance match improves from -27 dB to -44 dB at around 9.8 GHz. In Fig. 13(c) when W_1 is increased from 0.5 mm to 1.25 mm the isolation between the array's elements improves from -34 dB to -55 dB at around 9.8 GHz, and from -53 dB to notch -66.5 dB at around 10.65 GHz. The optimum value of W_1 is 1.25 mm.

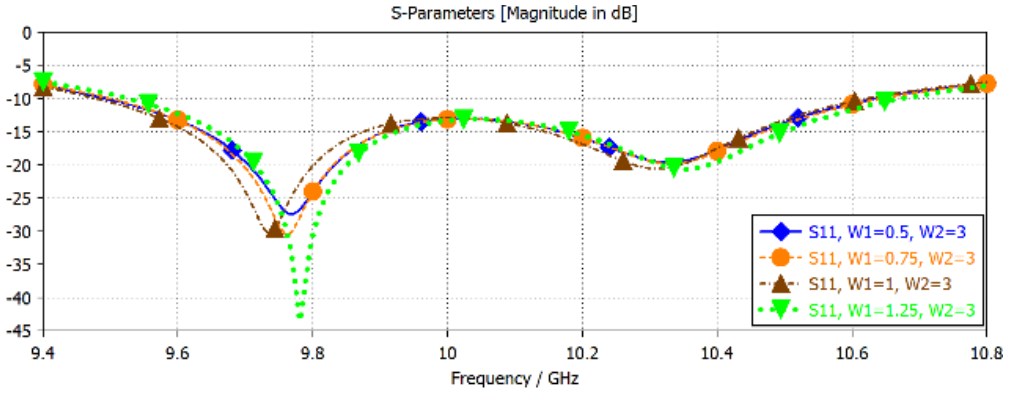

(a) Reflection-coefficient

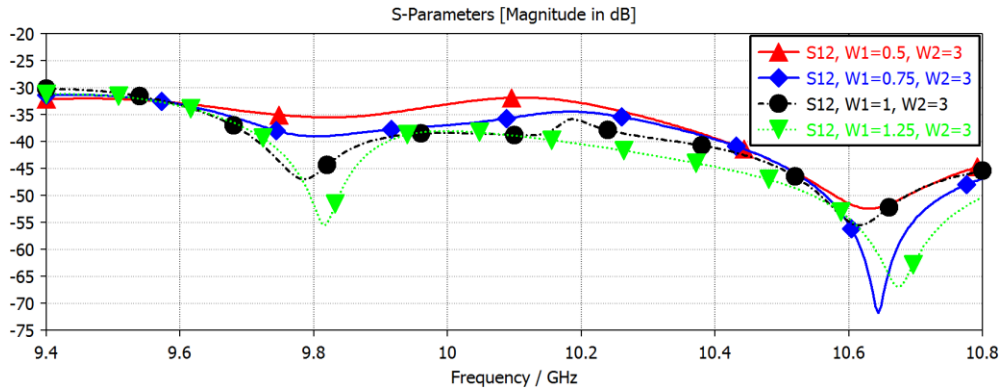

(b) Transmission-coefficient (S_{12})

Fig. 13. Parametric study on slit width (W_1) when the gap between the E-shaped slits is fixed at 3 mm.

B) Effect of Slit Gap

Fig. 14(a) & (b) shows the E-shape slit gap (W_2) has negligible effect on the reflection coefficient (magnitude and phase) response. Fig. 14(c) shows the isolation significantly improves at around 9.8 GHz and 10.6 GHz when W_2 is increased from 1 mm to 3 mm by 10 dB and 37 dB, respectively. When W_2 is increased to 4 mm the improvement diminishes due to overlapping between slot and edge of slab. The optimum gap is 3 mm.

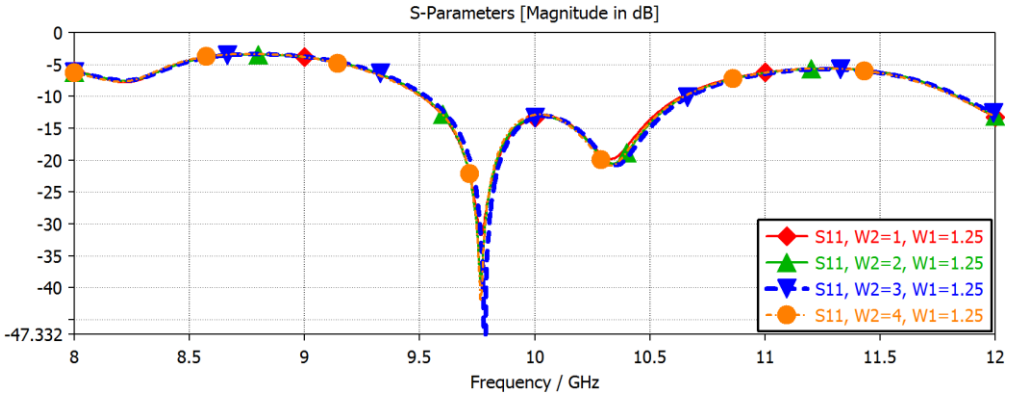

(a) Reflection-coefficient (S_{11})

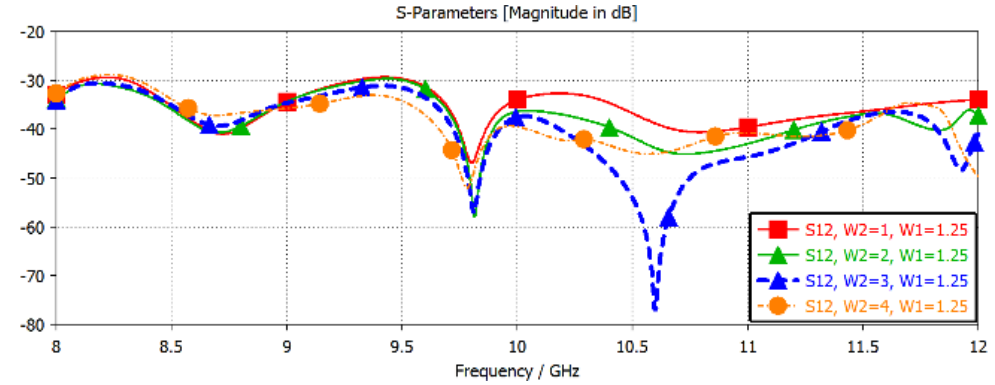

(b) Transmission coefficient (S_{12})

Fig. 14. Effect of gap between the E-shaped slits (W_2) when slit width (W_1) is fixed at 1.25 mm.

IV. Measured Results

Photograph of the patch antenna array without and with MTM-DS are shown in Fig. 15. The measured response of the reflection and transmission-coefficients is shown in Fig. 16. It shows the mutual coupling between radiating elements is reduced over a large frequency span from 9 GHz to 11 GHz using the proposed MM-DS. In fact, the measured isolation with MTM-DS at 9.95 GHz is -34 dB, at 10.25 GHz is -37 dB and at 10.85 GHz is -57 dB. However, without MTM-DS, the measured isolation at 9.95 GHz is -27 dB, at 10.25 GHz is -26 dB and at 10.85 GHz is -37 dB. The results show improvement in isolation from 9.4 GHz to 11 GHz. In addition, impedance matching is particularly good at f_{r_1}= 9.95 GHz and f_{r_2}= 10.63 GHz. At these frequencies, the isolation between elements is -34 dB and -34.8 dB, respectively. Measured S-parameter results are summarized in Table VI. Without MTM-DS the average isolation over 9 GHz to 11 GHz is -27 dB, and with MTM-DS it is -38 dB. On average the isolation is improved by 11 dB.

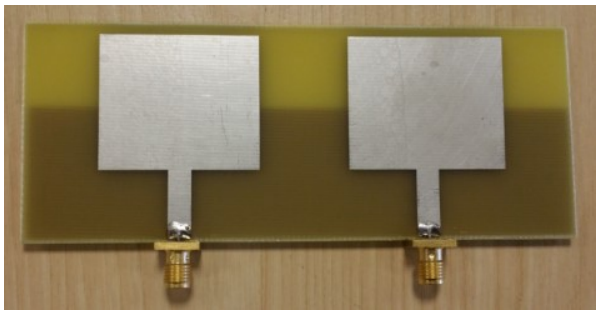

(a) Top view, without MTM-DS

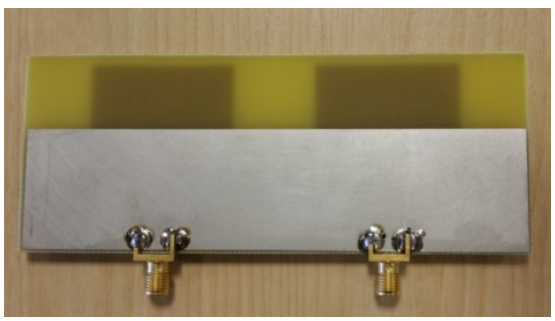

(b) Bottom view, without MTM-DS

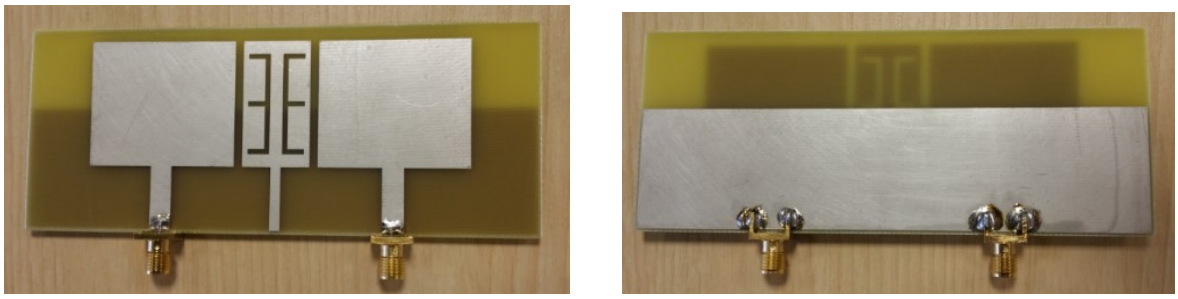

(c) Top view, with MTM-DS (d) Bottom view, with MTM-DS

Fig. 15. Photographs of the antenna array with no MTM-DS and with MTM-DS. The antenna array is constructed on FR-4 lossy substrate with thickness of h = 1.6 mm, dielectric constant of $\varepsilon_r = 4.3$ and $tan\delta = 0.025$.

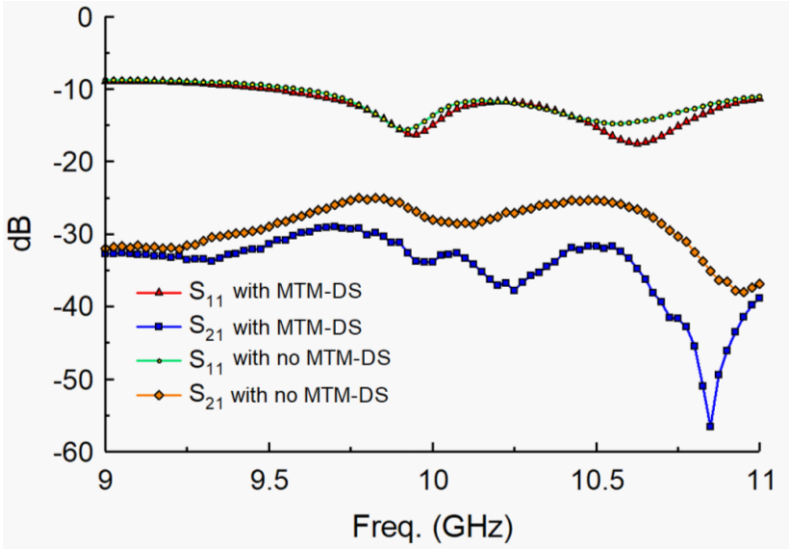

Fig. 16. Measured reflection-coefficient (S_{11}) and transmission-coefficient (S_{12}) response without and with MTM-DS.

TABLE VI: Measured Antenna Array Parameters

Bandwidth (BW) defined for S_{11}<-10 dB

Without MTM-DS	BW = 1.3 GHz (9.6 GHz – 10.9 GHz), Fractional bandwidth = 12.68%	@ f_{r_1} = 9.90 GHz impedance match = -16 dB	@ f_{r_2} = 10.55 GHz impedance match = -15 dB
With MTM-DS	BW = 1.6 GHz (9.4 GHz – 11.0 GHz), Fractional bandwidth = 15.68%	@ f_{r_1} = 9.95 GHz impedance match = -16 dB	@ f_{r_2} = 10.63 GHz impedance match = -18 dB

Mutual Coupling Suppression Between Adjacent Antennas (S_{12})

	Minimum	Average	Maximum
Without MTM-DS	-25 dB	-27 dB	-37 dB
With MTM-DS	-29 dB	-38 dB	-57 dB

V. Radiation Patterns of the Proposed Array Antenna

The measured 2-D radiation plots for the antenna array without and with MTM-DS at various frequencies are shown in Fig. 17. Also plotted is the simulated radiation pattern at 9.85 GHz, which shows good correlation with the measured plot at the same frequency. These plots show the effect of MTM-DS in the magnetic-plane is minimal. Although there is some effect in the electric-plane however this is not considerable. In fact, the gain is improved with MTM-DS at 9.85 GHz at an angle of 90 degrees. A standard anechoic chamber was used to measure the antenna's gain where a transmitting horn antenna was located at the focal point of the reflector to convert the spherical waves to plane waves directed towards the antenna under test (AUT). The antenna gain was measured using the standard comparative method with the antennas fed in-phase. Connector losses were considered in the measurements.

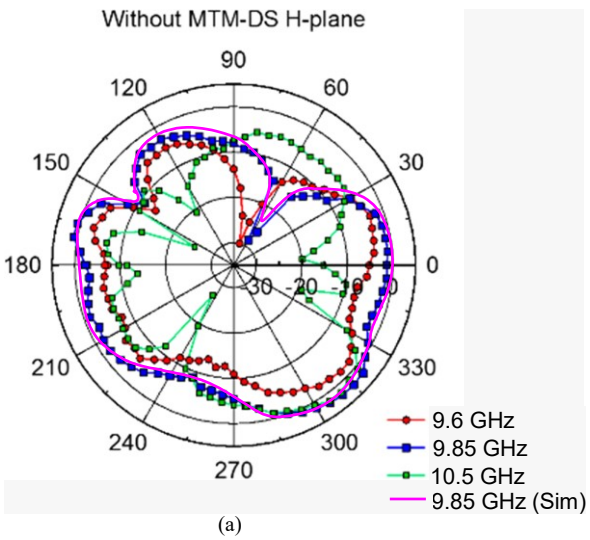

(a)

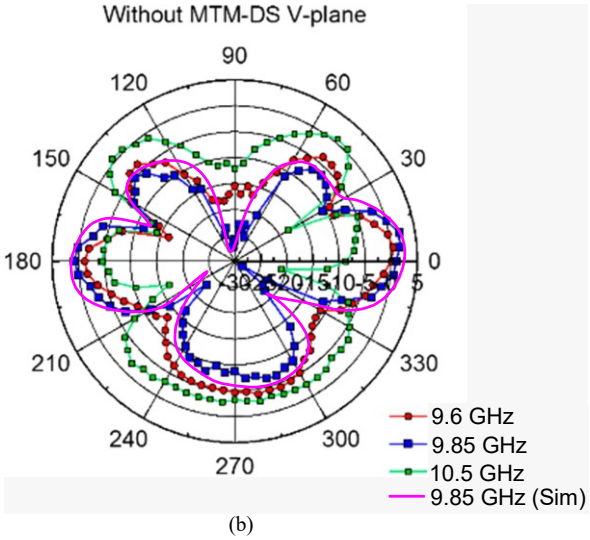

(b)

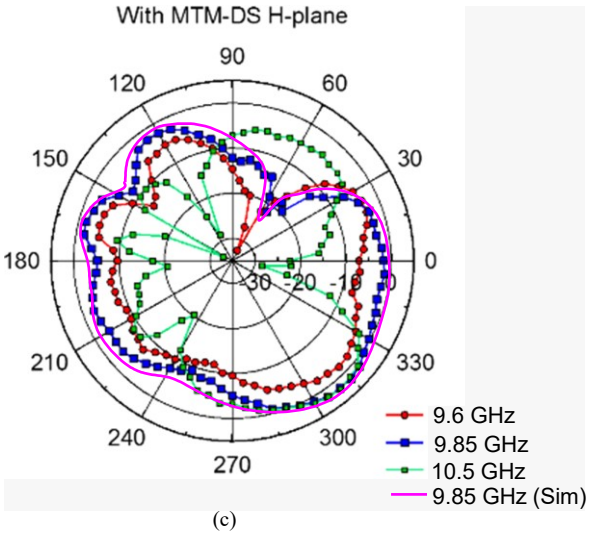

(c)

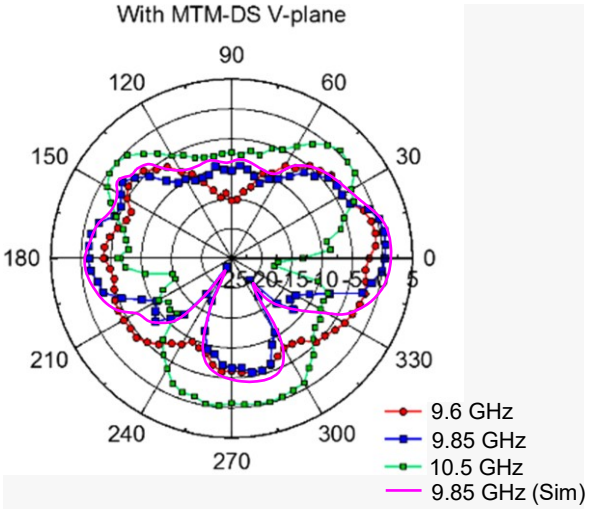

(d)

Fig. 17. Measured and simulated polar plots of the antenna array without and with MTM-DS at spot frequencies in magnetic (H) and electric (V) planes.

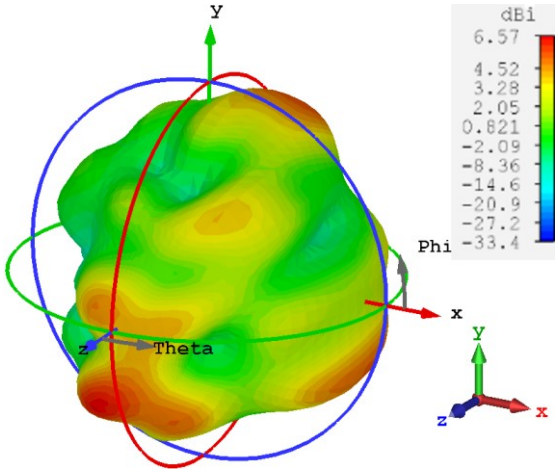

(a) @ 9.95 GHz without MTM-DS

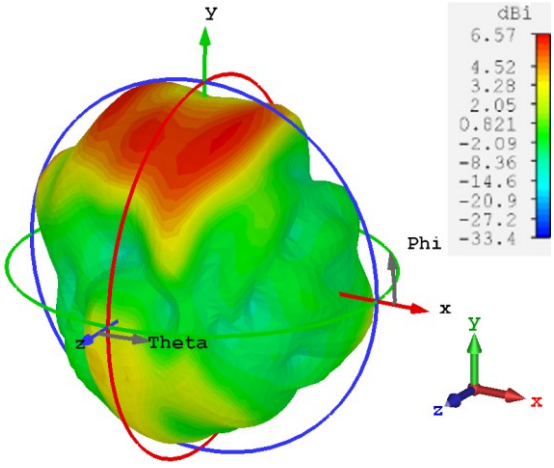

(b) @ 10.63 GHz without MTM-DS

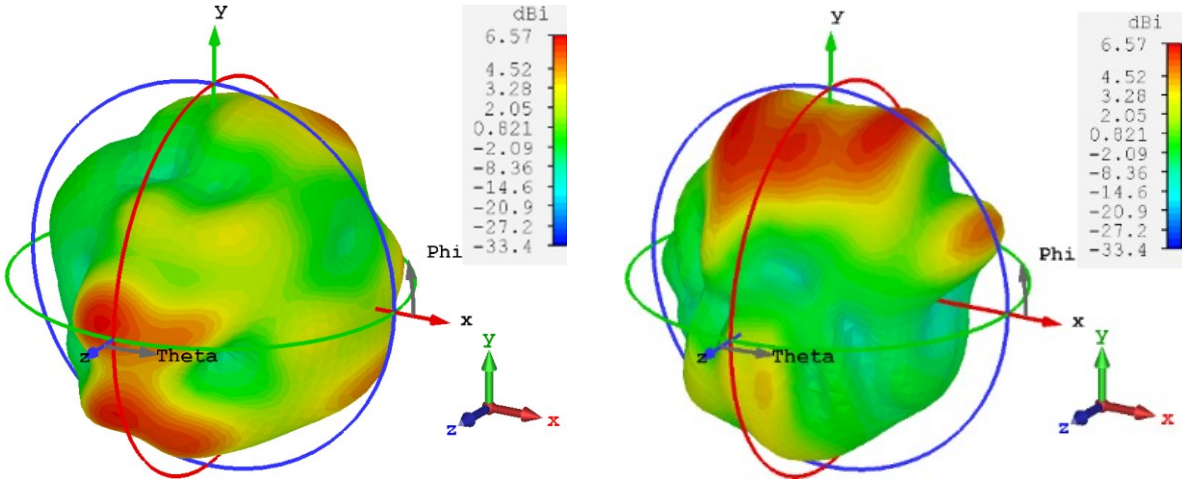

(c) @ 9.95 GHz with MTM-DS (d) @ 10.63 GHz with MTM-DS

Fig. 18. 3D radiation patterns without and with MTM-DS at high impedance matching frequencies.

The simulated 3D far-field radiation patterns at frequencies of high impedance match in Fig. 18 show there is good correlation without and with application of MTM-DS. These results confirm there is little impact with MTM-DS on the pattern specifications. It is also observed in Fig. 18 that the radiation patterns are more directive with the proposed MTM-DS. Gain at 9.95 GHz and 10.63 GHz are 4.31 dBi and 4.85 dBi, respectively, without MTM-DS; and 4.52 dBi and 5.40 dBi, respectively, after applying the MTM-DS.

Comparison of the proposed technique with other methods reported to date in Table VII. It is clear the proposed technique offers significantly higher mutual coupling suppression with closely spaced radiators and is relatively easy to construct and integrate in densely packed array antenna. It removes the drawback of poor front-to-back-ratio reported in other decoupling techniques. In addition to high-coupling suppression, the MTM-DS can be retrofitted subject to sufficient space between the antennas which makes this technique versatile for various applications having stringent performance requirements. One drawback of the proposed technique compared to [15] is that the radiation patterns is seriously affected over its wider operational bandwidth.

TABLE VII: Comparison of the Proposed Mutual Coupling Suppression Technique with Other Reported Techniques

Refs.	Mutual coupling suppression technique	Maximum mutual coupling suppression (dB)	Patch separation (λ_o)	Operating bandwidth reduction (%)	Design Complexity
[5]	Shorted annular elliptical patch (SAEP)	8	0.75	19	Moderate
[6]	Ring of magnetic current	10	0.5	13	Moderate
[12]	Complementary split-ring resonators (CSRR)	37	0.125	0	High
[13]	Complementary split-ring resonators (CSRR)	10	0.25	22	High
[15]	Complementary split-ring resonator (CSRR)	27	0.125	29	Low
[16]	U-shaped microstrip line	17	0.75	12	Moderate
[17]	Periodically grounded edge-coupled split-ring resonators (PGE-SRRs)	18	0.5	0	High
This work	MTM-DS	57	0.66	0	Low

VI. Conclusion

An effective technique is presented for suppressing mutual coupling encountered in antenna arrays. This involves inserting MTM-DS between the radiating elements. With the proposed technique the edge-to-edge separation between the antennas in the antenna array can be reduced to $0.66\lambda_o$, where the free-space wavelength is at 10 GHz. MTM-DS comprises two E-shaped slits arranged in a mirror image that are engraved on a rectangular patch. MTM-DS is shown to effectively minimise mutual coupling between adjacent radiators by suppressing surface wave propagation. With the proposed MTM-DS the mutual coupling suppression on average is -38 dB over 9 GHz to 11 GHz.

ACKNOWLEDGMENTS

This work is partially supported by innovation programme under grant agreement H2020-MSCA-ITN-2016 SECRET-722424 and the financial support from the UK Engineering and Physical Sciences Research Council (EPSRC) under grant EP/E022936/1. With reference to this work readers can contact Mr. M. Alibakhshikenari by sending an email to alibakhshikenari@ing.uniroma2.it.

REFERENCES

[1] Pan, B.C., Tang, W.X., Qi, M.Q., et al (2016), Reduction of the spatially mutual coupling between dual-polarized patch antennas using coupled metamaterial slabs, *Nat. Sci. Rep*., 6, 1–8.

[2] Al-Hasan, M.J., Denidni, T.A., and Sebak, A.R. (2015), Millimeter-wave compact EBG structure for mutual coupling reduction applications, *IEEE Trans. Antennas Propag*., 63(2), 823–828.

[3] Bernety, H.M., and Yakovlev, A.B. (2015), Reduction of mutual coupling between neighboring strip dipole antennas using confocal elliptical metasurface cloaks, *IEEE Trans. Antennas Propag*., 63(4), 1554–1563.

[4] James, J.R., Henderson, A. (1979), High-frequency behavior of microstrip open-circuit terminations. *IEE J. Microw. Opt. Acoust*., 3(9), 205–218.

[5] Amendola, G., Boccia, L., Massa, G. (2005), Shorted elliptical patch antennas with reduced surface waves on two frequency bands, *IEEE Trans. Antennas Propag*., 53(6), 1946– 1956.

[6] Jackson, D.R., Williams, J.T., Bhattacharyya, A.K., Smith, R.L., Buchheit, S.J., Long, S.A. (1993), Microstrip patch designs that do not excite surface waves, *IEEE Trans. Antennas Propag*., 41(8), 1026– 1037.

[7] Yang, L., Fan, M.Y., Chen, F.L., She, J.Z., Feng, Z.H. (2005), A novel compact electromagnetic bandgap structure and its applications for microwave circuits, *IEEE Trans. Microw. Theory Tech*., 53(1), 183– 190.

[8] Guha, D., Biswas, S., Joseph, T., Sebastian, M.T. (2008), Defected ground structure to reduce mutual coupling between cylindrical dielectric resonator antennas, *Electron. Lett*., 44(14), 836– 837.

[9] Liu, H., Li, Z., Sun, X., Mao, J. (2005), Harmonic suppression with photonic bandgap and defected ground structure for a microstrip patch antenna, *IEEE Microw. Compon. Lett*., 15(2), 55– 56.

[10] Ting, S.-W., Tam, K.-W., Martins, R.P. (2006), Miniaturized microstrip lowpass filter with wide stopband using double equilateral U-shaped defected ground structure, *IEEE Microw. Compon. Lett*., 16(5), 240– 242.

[11] Guha, D., Biswas, S., Biswas, M., Siddiqui, J.Y., Antar, Y.M.M. (2006), Concentric ring-shaped defected ground structures for microstrip applications, *IEEE Antennas Wirel. Propag. Lett*., 5(1), 402–405.

[12] Shafique, M.F., Qamar, Z., Riaz, L., Saleem, R., and Khan, S.A., (2015), Coupling suppression in densely packed microstrip array using metamaterial structure, *Microw. Opt. Technol. Lett*., 57(3), 759–763.

[13] Wahid, A., Sreenivasan, M., and Rao, P.H., (2015), CSRR loaded microstrip array antenna with low side lobe level, *IEEE Antennas Wireless Propag. Lett.*, 14, 1169–1171.

[14] Qamar, Z., Riaz, L., Chongcheawchamnan, M., Khan, S.A. and Shafique, M.F., (2014), Slot combined complementary split ring resonators for mutual coupling suppression in microstrip phased arrays, *IET Microw. Antennas Propag*., 8(15), 1261–1267.

[15] Qamar, Z., Naeem, U., Khan, S.A., Chongcheawchamnan, M, and Shafique, M.F., (2016), Mutual coupling reduction for high-performance densely packed patch antenna arrays on finite substrate, *IEEE Trans. Antennas Propag*., 64(5), 1653-1660.

[16] Farsi, S. Aliakbarian, H., Schreurs, D., Nauwelaers, B., and Vandenbosch, G.A. (2012), Mutual coupling reduction between planar antennas by using a simple microstrip U-section, *IEEE Antennas Wireless Propag. Lett*., 11, 1501–1503.

[17] Tang, M.C., Xiao, S., Wang, B, Guan, J., and Deng, T. (2011), Improved performance of a microstrip phased array using broadband and ultra-low loss metamaterial slabs, *IEEE Antennas Propag. Mag*., 53(6), 31–41.

[18] Hafezifard, R., Naser-Moghadasi, M., Mohassel, J.R., Sadeghzadeh, R.A. (2016), Mutual coupling reduction for two closely spaced meander line antennas using metamaterial substrate, *IEEE Antennas & Wireless Propag. Lett*., 15, 40 – 43.

[19] Chang, K, Hsieh, L.-H., Microwave Ring Circuits and Related Structures, Wiley.

[20] Paul, L. C., et al., (2017), Design a slotted metamaterial microstrip patch antenna by creating three dual isosceles triangular slots on the patch and bandwidth enhancement, *Int. Conf. on Electrical Information and Communication Technology* (EICT), 1-6.

[21] Yu, B., eta al., (2017), Metamaterial-based low-profile broadband hexagonal-grid-slotted patch antenna, *Int. Applied Computational Electromagnetics Society Symposium* (ACES), 1-2.

[22] Pyo, S., J.-W. Baik, S.-H. Cho and Y.-S. Kim, (2009), Metamaterial-based antenna with triangular slotted ground for efficiency improvement, *Electronics Letters*, 45(3), 144-146.

[23] Caloz, C., Itoh, T., (2005), Electromagnetic Metamaterials: Transmission Line Theory and Microwave Applications, Wiley

[24] Smith, D.R., Vier, D.C., Koschny, T., Soukoulis, C.M. (2005), Electromagnetic parameter retrieval from inhomogeneous metamaterials, *PHYSICAL REVIEW* E 71, 036617.